Geochemical Perspectives Letters

© 2024 The Authors
Published by the European Association of Geochemistry

$^{238}U/^{235}U$ in deep-sea corals reflects limited expansion of seafloor anoxia in last ice age

M.A. Kipp[1,†*], A. Gao[1], J.F. Adkins[2], F.L.H. Tissot[1]

OPEN ACCESS

https://doi.org/10.7185/geochemlet.2449

Abstract

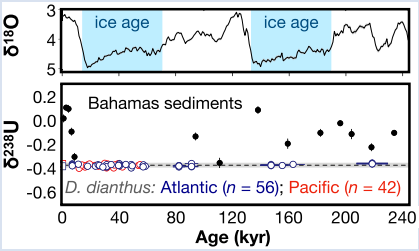

Although much evidence suggests a decrease in deep ocean oxygen levels during the last glacial period, a quantitative global constraint on anoxic *versus* suboxic seafloor area is still lacking. Establishing such a constraint is challenging, because while changes in the biological pump are thought to drive deep ocean oxygen depletion during glacial time, concurrent changes in sea level and ocean circulation may have variable effects on the prevalence of anoxia on continental shelves. Here we use the uranium isotope redox proxy in cold-water corals to constrain anoxic seafloor area over the last 220 kyr. All samples show modern-like $\delta^{238}U$ values within tight bounds (<0.05 ‰), allowing very little change in anoxic seafloor over this interval. This contrasts with coeval carbonate sediments that show large $\delta^{238}U$ variations due to diagenetic alteration. It also contrasts with other redox proxy records, including authigenic uranium enrichments and sedimentary thallium isotopes, that show evidence of glacial oxygen depletion. We conclude that while the glacial ocean experienced an expansion of deep water suboxia, global seafloor anoxia remained roughly constant.

Received 16 August 2024 | Accepted 9 December 2024 | Published 23 December 2024

Introduction

Atmospheric CO_2 levels have fluctuated across Quaternary glacial-interglacial cycles. During the shift from the Last Glacial Maximum (LGM) to the Holocene, an ~80 ppm CO_2 increase was accompanied by several degrees of global mean temperature increase, >100 m of sea level rise, and a collapse of continental ice sheets (Shakun *et al.*, 2012). Understanding the mechanism(s) controlling these climatic changes is critical for many reasons, foremost being concern about climatic effects of anthropogenic CO_2 emissions (>120 ppm) that have already exceeded the increase from the LGM to Holocene.

To explain large pCO_2 swings on kyr timescales, most studies invoke carbon movement between the atmosphere and ocean. While originally an increase in productivity was proposed as a means of marine carbon sequestration (Broecker, 1982), subsequent work invoked a more efficient biological pump (*i.e.* nutrients more completely utilised), particularly at high latitudes (Sarmiento and Toggweiler, 1984). When coupled with ocean circulation changes, a more efficient biological pump would prevent carbon leakage from the deep ocean to atmosphere, namely in the Southern Ocean (Sigman and Boyle, 2000), thereby lowering pCO_2. Although the processes responsible for an increase in biological pump efficiency remain debated, the consensus is that such variations can explain much of the pCO_2 variations across glacial cycles (Sigman *et al.*, 2010).

Importantly, this mechanism implies a stoichiometric increase in oxygen consumption from respiration in the water column, suggesting an oxygen deficit in glacial deep waters (Keir, 1988). Studies of pelagic settings have consistently found evidence of glacial oxygen depletion, but not benthic anoxia (reviewed in Jacobel *et al.*, 2020). In contrast, studies of continental margins – which host the majority of anoxic seafloor today – paint a more complicated picture. In some currently anoxic settings, bottom waters were more oxygenated in glacial time (*e.g.*, Cariaco Basin; Yarincik *et al.*, 2000). Other sites show the opposite, experiencing oxygen depletion (*e.g.*, Namibian margin; Riedinger *et al.*, 2021). Further complicating things, glacioeustatic sea level changes altered the area of anoxic deposition *via* marine incursion into lacustrine settings during deglaciation, with the Black Sea providing a notable example (Arthur and Dean, 1998). Therefore, across glacial cycles the competing effects of productivity, sea level, ocean circulation, and temperature may have resulted in different changes in benthic anoxia across sites, making individual localities poor approximators of the global prevalence of seafloor anoxia. These confounding factors thwart global extrapolations of local records to such an extent that an understanding of the magnitude and sign of changes in seafloor anoxia across glacial cycles is still lacking.

Uranium isotopes ($^{238}U/^{235}U$, expressed in delta notation as $\delta^{238}U$) are a well established quantitative tracer of global ocean redox. Uranium (U) has a long marine residence time (~400 kyr; Ku *et al.*, 1977), making it well mixed and isotopically homogenous in seawater (Cheng *et al.*, 2000; Tissot and Dauphas, 2015; Kipp *et al.*, 2022). Furthermore, marine U isotope mass balance is dominated by preferential ^{238}U burial in reducing

1. The Isotoparium, Division of Geological and Planetary Sciences, California Institute of Technology, Pasadena, CA 91125, USA
2. Division of Geological and Planetary Sciences, California Institute of Technology, Pasadena, CA 91125, USA
† Present address: Division of Earth and Climate Sciences, Nicholas School of the Environment, Duke University, Durham, NC 27708, USA
* Corresponding author (email: michael.kipp@duke.edu)

sediments (Tissot and Dauphas, 2015; Andersen *et al.*, 2016). Thus, expansion of the "reduced" sink (*i.e.* expansion of anoxic seafloor area) will decrease seawater $\delta^{238}U$ ($\delta^{238}U_{sw}$). If one can access a record of $\delta^{238}U_{sw}$ through time, this can be equated to seafloor anoxia *via* isotope mass balance (*e.g.*, Kipp and Tissot, 2022). Carbonate sediments (review in Zhang *et al.*, 2020), and biological carbonate precipitates in particular (Chen *et al.*, 2018a; Kipp *et al.*, 2022), have been shown to record $\delta^{238}U_{sw}$, and have been extensively targeted in palaeo-redox studies.

Here, we use the $\delta^{238}U$ redox proxy to quantify changes in seafloor anoxia across glacial cycles. We leverage a well preserved, high resolution biological carbonate archive: cold-water scleractinian corals. These corals are faithful archives of $\delta^{238}U_{sw}$ (Kipp *et al.*, 2022) and their fossil record spans >200 kyr. We performed physical and chemical cleaning tests to ensure removal of exogenous U from fossil corals, then analysed a large fossil dataset. Our analyses ($n = 98$) reveal a narrow range of $\delta^{238}U$ values, which *via* isotope mass balance implies little change in anoxic seafloor area across the LGM. We compare this record to other redox proxies and make the argument that while anoxic area changed little across glacial time, suboxia likely became more prevalent in pelagic deep ocean settings.

Results

The 32 subsamples of eight corals subjected to variable cleaning treatments have nearly identical $\delta^{238}U$ values, between -0.402 ± 0.021 ‰ and -0.361 ± 0.029 ‰ (Fig. 1). All modern and fossil corals (Fig. 2) have $\delta^{238}U$ values within uncertainty of the salinity-normalised global average modern seawater value (-0.379 ± 0.023 ‰; Tissot and Dauphas, 2015; Kipp *et al.*, 2022). In contrast, $\delta^{234}U_i$ was anomalously high in one sample (+184.16 ‰) and low in another (+112.51 ‰) (Fig. 1). The $\delta^{238}U$ stability of the coral dataset contrasts with the considerable isotopic variability seen in coeval carbonate sediments (Chen *et al.*, 2018b; Tissot *et al.*, 2018).

Discussion

Impact of physical and chemical cleaning on coral U isotope ratios. As small $\delta^{238}U$ fluctuations could imply significant changes in seafloor anoxia, we examined the sensitivity of coral U isotope analyses to chemical cleaning. Over time, fossil deep-sea corals develop FeMn oxide coatings, which adsorb trace elements and potentially contaminate skeletal analyses if not removed. FeMn coatings are particularly problematic for

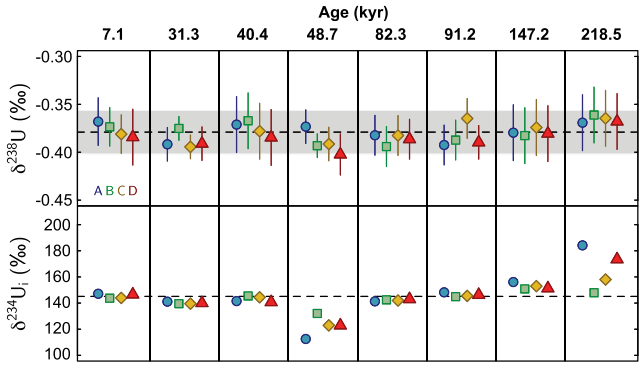

Figure 1 Impact of chemical cleaning on U isotopes. Treatments A-D are described in the Supplementary Information. No systematic relationships exist between U isotope ratios and chemical cleaning.

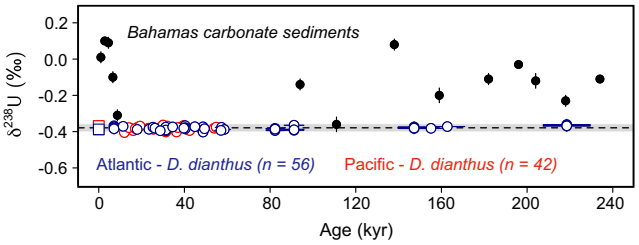

Figure 2 $\delta^{238}U$ in carbonate sediments and corals through the last 240 kyr. Black symbols denote Bahamas sediments (Tissot *et al.*, 2018). Red and blue circles denote *D. dianthus* from Pacific and Atlantic Ocean, respectively (this study). Red and blue squares denote modern seawater values for Pacific and Atlantic, respectively. Grey band denotes modern global average $\delta^{238}U_{sw}$ (Kipp *et al.*, 2022).

U-series dating, as their Th content is much higher than coral skeletons (Cheng *et al.*, 2000).

There is a long history of chemical cleaning of corals before trace element analysis (*e.g.*, Shen and Boyle, 1988; Lomitschka and Mangini, 1999; Cheng *et al.*, 2000). We consolidated some of these practices into a series of tests (Table S-5; Supplementary Information) that were applied to subsamples (septa with some thecal material) from eight corals of varying ages. The tests spanned minimal to intensive oxidative cleaning; reductive cleaning was not studied here.

The $\delta^{238}U$ and $\delta^{234}U_i$ values were not affected by cleaning (Fig. 1). There are several possible reasons for this. First, all subsamples were subjected to extensive physical cleaning with a Dremel tool and/or scalpel. This removes most exogenous material (FeMn coatings, organics, detritus, secondary carbonate), leaving little to be removed *via* chemical cleaning (confirmed by elemental analyses; Fig. S-3). Second, U concentrations are similar in crust and coral material (Cheng *et al.*, 2000). Thus, by physically removing most of the coating, the signal is overwhelmed by coral U. This is in contrast to Th, which is $\sim 10^4$ times more concentrated in coatings (Cheng *et al.*, 2000). Third, because we aimed to recover 100–1000 ng U for high precision $\delta^{238}U$ analysis, we digested large samples (10s to 100s mg). This gives a lower surface area to volume ratio than samples cut from surface layers of septa, buffering against exogenous U contributions. Overall, we concluded that U isotope analyses of fossil corals need not include chemical cleaning, and only performed physical cleaning for the remaining analyses.

Comparison of coral and carbonate sediment records. Over the last 240 kyr, $\delta^{238}U$ values in Bahamian carbonate sediment cores vary by >0.5 ‰ (Fig. 2; Romaniello *et al.*, 2013; Chen *et al.*, 2018b; Tissot *et al.*, 2018). This variation, which is predominantly attributed to diagenetic ^{238}U enrichment under reducing porewater conditions, has prevented the reconstruction of primary $\delta^{238}U_{sw}$ in the recent past. The tight range of coral $\delta^{238}U$ values (<0.05 ‰) observed here shows that $\delta^{238}U_{sw}$ was invariant over glacial time. This serves as a baseline from which the magnitude of diagenetic $\delta^{238}U$ offsets can be quantified. This record of constant $\delta^{238}U_{sw}$, coupled to the noisy record from Bahamian sediments, reinforces the conclusion that $\delta^{238}U_{sw}$ reconstructions using carbonate sediments are subject to considerable uncertainty due to not only the magnitude, but more so the variability of diagenetic alteration through stratigraphic sections (Kipp and Tissot, 2022).

Model constraints on anoxic and suboxic seafloor area. Our $\delta^{238}U$ record allows us to constrain changes in the area of anoxic and suboxic seafloor during glacial time. Using the inverse

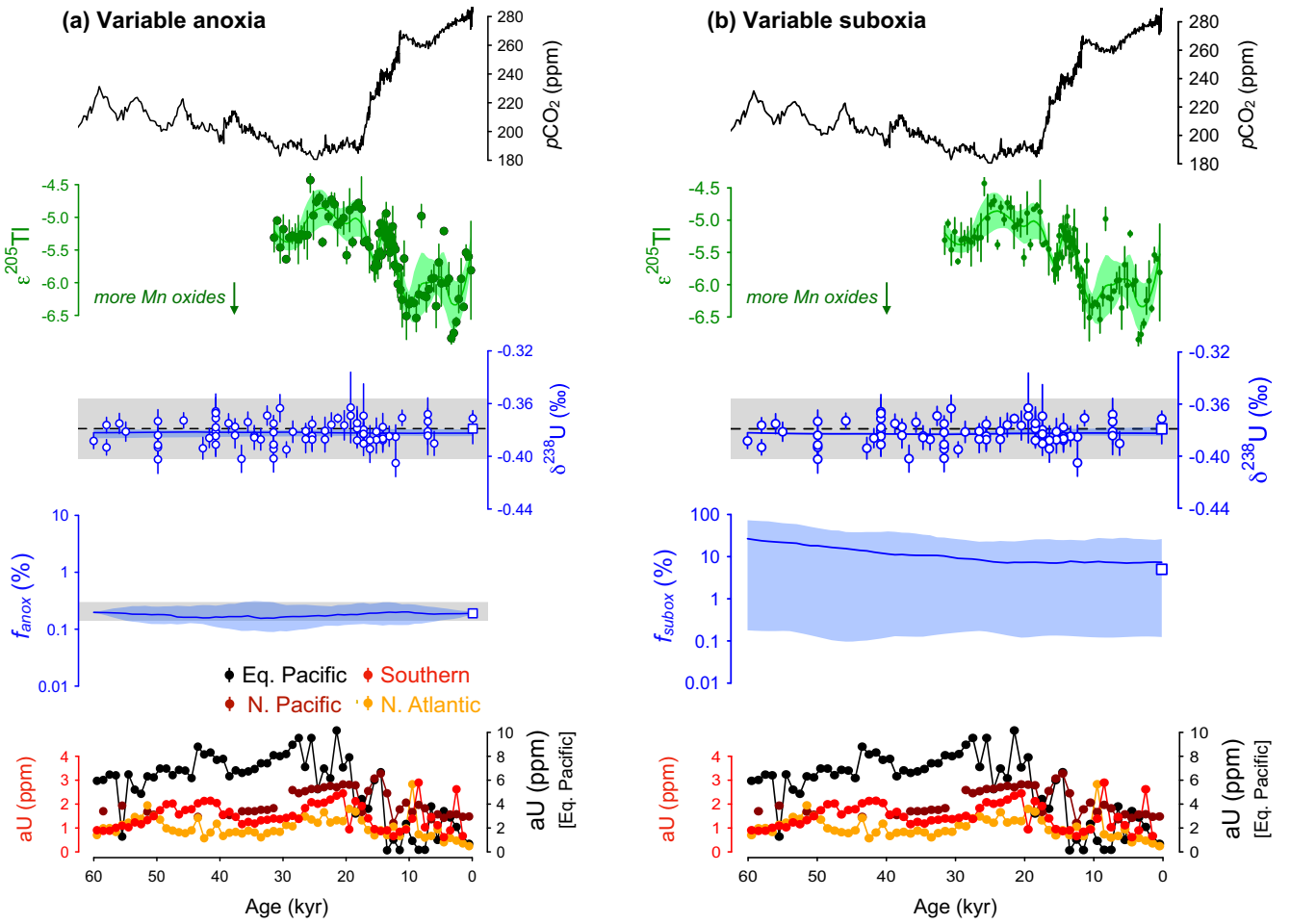

Figure 3 Reconstructed seafloor **(a)** anoxia (f_{anox}) or **(b)** suboxia (f_{subox}) through the last 60 kyr. CO_2 (black lines) from Antarctic ice core composite (NOAA); Tl isotopes (green points) from Wang *et al.* (2024) with LOESS trendline and 2σ confidence interval; basin-averaged authigenic U (aU) from sources in Table S-9). Reconstructed f_{anox} and f_{subox} plotted as median (lines) and 16th to 84th percentile confidence intervals (shading).

isotope mass balance model of Kipp and Tissot (2022), we explored the last 60 kyr of our record where data density is highest. We find that the median reconstructed extent of seafloor anoxia (f_{anox}) through the 60 kyr record is within uncertainty of the modern value (Fig. 3a), with 84 % confidence that f_{anox} never exceeded 0.3 % (the upper limit on modern estimate; grey shading in Fig. 3a).

A few takeaways emerge from this stringent redox constraint. First, it invalidates models of glacial ocean chemistry (*e.g.*, Broecker, 1982) that imply deep ocean anoxia due to a stronger biological pump and slower ocean circulation. While such models have fallen out of favour and been superseded by models invoking deep ocean suboxia, our finding strengthens that consensus. To further illustrate an upper limit on redox change, we performed forward model tests where f_{anox} (modern = 0.2 %) was increased to 1 %, 2 % and 5 % during the LGM (25 to 18 ka). These yield $\delta^{238}U_{sw}$ trajectories (Fig. 4a) that increasingly deviate from the coral $\delta^{238}U$ record, firmly suggesting that f_{anox} did not exceed 1 % during glacial time. Compared to "anoxic events" in Earth's past, which the $\delta^{238}U$ proxy implies have experienced f_{anox} of up to tens of percent over 100s of kyr (Zhang *et al.*, 2020; Kipp and Tissot, 2022), the glacial ocean experienced a much subtler redox change that did not impact $\delta^{238}U_{sw}$.

Second, glacial-interglacial dynamics in individual low-oxygen settings can be tested against this constraint. For instance, the Black Sea, which today represents roughly half of anoxic seafloor area, became isolated from the ocean during glacial time, with marine re-connection at ~9 ka (Arthur and Dean, 1998). Its isolation and re-connection to the ocean could, in principle, impact f_{anox}. Model runs simulating the re-connection of the Black Sea, however, show no visible changes in $\delta^{238}U_{sw}$ on the timescale available (Fig. 4b). The reason for the difference between this and the prior test (Fig. 4a) is that excursions to higher than modern f_{anox} result in rapid $\delta^{238}U_{sw}$ changes (due to rapid U scavenging from seawater in anoxic settings), whereas deviations toward lower than modern f_{anox} have much smaller and slower effects (due to the slow trend toward crustal $\delta^{238}U$ from the trickle of riverine U into the ocean).

Third, we considered how possible changes in global runoff during deglaciation might affect the U flux into seawater. We tested this by arbitrarily doubling riverine U input (J_{riv}) during deglaciation (as well as exploring a concurrent change in isotopic composition), finding that there would not be significant effects on $\delta^{238}U_{sw}$ (Fig. 4d). The reason, as above, is that riverine U inputs are small compared to the size of the marine reservoir. Thus, even doubling J_{riv} would not significantly affect $\delta^{238}U_{sw}$ on 10 kyr timescales.

Last, we considered a set of tests incorporating a third sink: "suboxic" sediments. While most work with the $\delta^{238}U$ proxy uses a simplified scheme of anoxic *vs.* non-anoxic sinks, U burial occurs on a continuum that includes "suboxic" sediments (Morford and Emerson, 1999), *i.e.* those with O_2 in

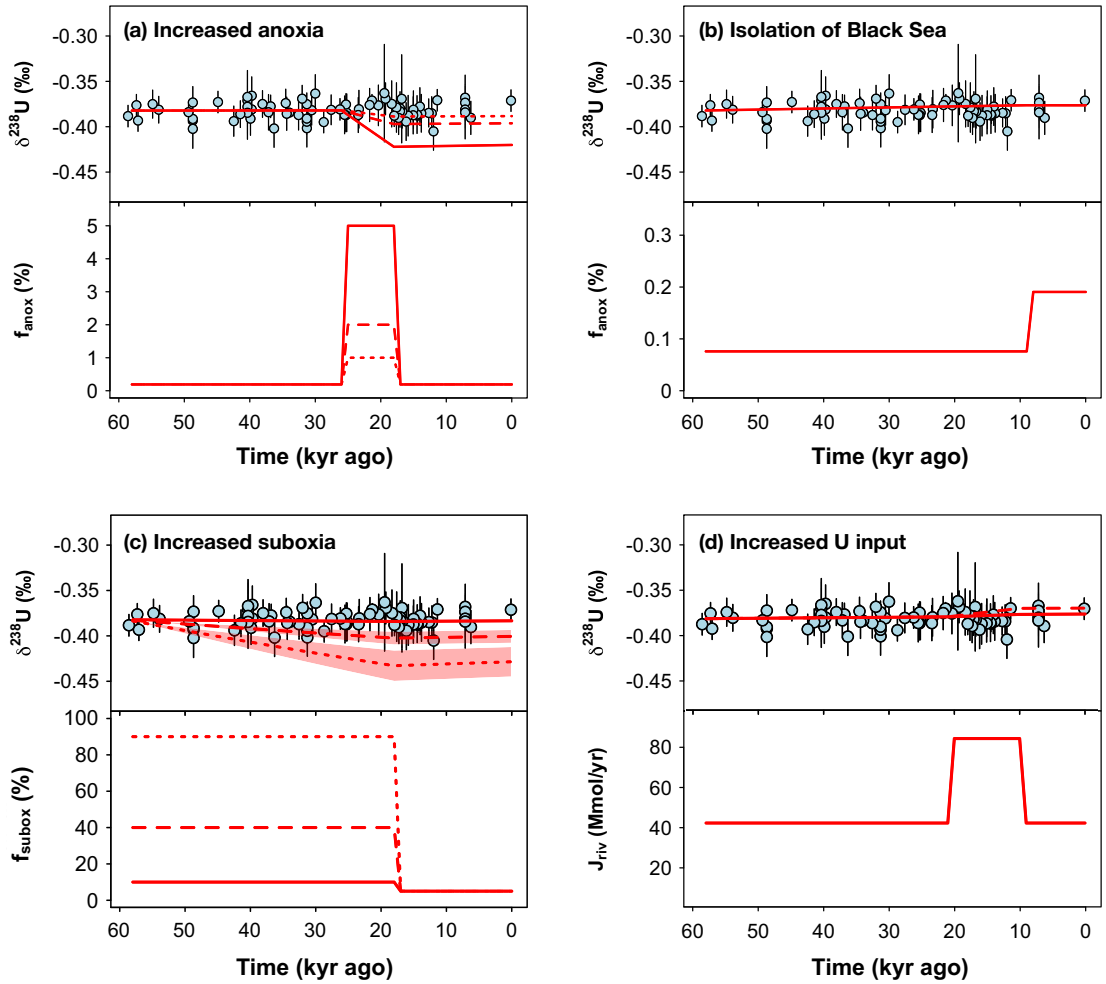

Figure 4 Forward model experiments. **(a)** Large f_{anox} change during LGM, **(b)** change in f_{anox} due to isolation of Black Sea, **(c)** large change in f_{subox}, **(d)** change in J_{riv} during deglaciation. Shading in **(c)** denotes range of Δ_{subox} from 0.1 to 0.2 ‰. Dashed line in **(d)** denotes run with $\delta^{238}U_{riv} = -0.15$ ‰ from 20 to 10 ka. In all tests, model forcing (bottom panels) ends at modern value.

bottom waters but O_2 depletion in shallow porewaters (we note that this definition of "suboxic" differs from some used in the literature; see, *e.g.,* Canfield and Thamdrup, 2009; for isotope mass balance purposes, "suboxic" simply means a sink with intermediate rate constant and isotopic effect). The expressed U isotopic fractionation during burial in "suboxic" settings is a matter of open debate; while sensitive to factors such as sedimentation rate and organic export (*e.g.,* Lau *et al.,* 2020), we here adopted $\Delta_{subox} = 0.1$ ‰ (Tissot and Dauphas, 2015; Andersen *et al.,* 2016) and a scavenging rate between those of anoxic and oxic sediments. We performed an inversion where the suboxic sink was added and f_{anox} was held at the modern value. We found that a wide range of f_{subox} values was consistent with the $\delta^{238}U$ record (Fig. 3b). The reason for the lack of constraint is that this sink has little leverage on $\delta^{238}U_{sw}$ due to the small isotopic effect and lower scavenging coefficient than anoxic settings. While both of those values are uncertain, this test reveals an important point: suboxic settings may have become more prevalent during glacial time without leaving an imprint on $\delta^{238}U_{sw}$. Below, we consider evidence that supports an expansion of glacial deep ocean suboxia and reconcile it with our $\delta^{238}U$ record.

Expansion of deep ocean suboxia, but not anoxia. Several lines of evidence point to lower oxygen in glacial deep waters; here we focus on two proxies relevant to our $\delta^{238}U$ dataset: authigenic uranium (aU) and thallium isotopes ($\varepsilon^{205}Tl$). Authigenic uranium enrichments have long been recognised in glacial marine sediments (*e.g.,* Chase *et al.,* 2001). While aU is higher under more reducing conditions (and can be achieved under suboxia, not just anoxia), it is also sensitive to export production and sedimentation rate (McManus *et al.,* 2005). Compilations of aU for the last glacial show strong inter-site differences, related to productivity and sedimentation rate, as well as changes in ocean circulation. On top of this heterogeneity is "burndown" of aU peaks during oxidation of older sediments. Despite these complexities, basin scale compilations consistently show greater aU at the LGM than Holocene (*e.g.,* North Pacific, Jaccard and Galbraith, 2013; Equatorial Pacific, Jacobel *et al.,* 2020; North Atlantic, Zhou and McManus, 2023).

While global extrapolation from these local records is uncertain, we conducted a sensitivity test to determine whether our $\delta^{238}U$ record precludes a glacial expansion of seafloor suboxia. We assigned $f_{subox} = 10$, 40 and 90 % during the last glacial and varied Δ_{subox} between 0.1 and 0.2 ‰. We see that f_{subox} up to ~40 % has little impact on $\delta^{238}U_{sw}$ (Fig. 4c), meaning changes in f_{subox} – that potentially gave rise to observed aU enrichments – are allowable given the $\delta^{238}U$ data. This is consistent with Figure 3b and highlights the insensitivity of $\delta^{238}U$ to suboxia on glacial timescales.

We also consider a new, purportedly global record of glacial ocean redox: Tl isotopes in reducing sediments. Cores TN041-8PG/8JPC from the Oman margin revealed a $\varepsilon^{205}Tl$ trend (Fig. 3) that suggests a shift from more reducing to more

oxidising deep ocean conditions during the last deglaciation (Wang *et al.* 2024). Marine Tl isotope mass balance is mainly affected by Tl adsorption to Mn oxides in oxygenated waters. Thus, glacial expansion of deep ocean suboxia could have diminished the impact of this sink, causing higher ε^{205}Tl. As demonstrated above, this would have little effect on $\delta^{238}U_{sw}$.

Conclusions

Our data imply minimal change in anoxic seafloor area during the last ice age, but allow significant changes in seafloor suboxia. In view of other proxy records, expansion of suboxic sediment area appears probable, particularly in the pelagic deep ocean. Though our record cannot quantify pelagic suboxia, recent efforts to do so (*e.g.*, Jacobel *et al.*, 2020) have concluded that observed water column oxygen deficits imply stoichiometric amounts of dissolved inorganic carbon storage that can explain much of the glacial CO_2 drawdown. Our data are consistent with these estimates, and thus are consistent with the biological pump playing an important role in glacial marine carbon sequestration.

As for continental shelves, our results require that settings with local expansion of glacial anoxia, or even euxinia (*e.g.*, Namibian shelf), were mostly balanced by locations that became better oxygenated (*e.g.*, Cariaco Basin), or disconnected from the ocean (*e.g.*, Black Sea). Modest change in f_{anox} is possible, but more likely toward lower than higher values. Our forward model experiments imply a strict upper limit on f_{anox} of ~1 %, but our inverse analyses of the coral $\delta^{238}U$ timeseries make a probabilistic case for even less variability (<16 % likelihood of f_{anox} >0.3 % at any point in the last 60 kyr). Future work could corroborate these estimates with more thorough compilations of varved sediment area through time.

Acknowledgements

This work was supported by a Postdoctoral Fellowship in Geobiology from the Agouron Institute to MAK, a Caltech WAVE Fellowship to AG, as well as NSF grant MGG-2054892, a Packard Fellowship, a research award from the Heritage Medical Research Institute, and start-up funds (provided by Caltech) to FLHT.

Editor: Gavin Foster

Additional Information

Supplementary Information accompanies this letter at https://www.geochemicalperspectivesletters.org/article2449.

© 2024 The Authors. This work is distributed under the Creative Commons Attribution Non-Commercial No-Derivatives 4.0 License, which permits unrestricted distribution provided the original author and source are credited. The material may not be adapted (remixed, transformed or built upon) or used for commercial purposes without written permission from the author. Additional information is available at https://www.geochemicalperspectivesletters.org/copyright-and-permissions.

Cite this letter as: Kipp, M.A., Gao, A., Adkins, J.F., Tissot, F.L.H. (2024) $^{238}U/^{235}U$ in deep-sea corals reflects limited expansion of seafloor anoxia in last ice age. *Geochem. Persp. Let.* 33, 32–37. https://doi.org/10.7185/geochemlet.2449

References

Andersen, M.B., Vance, D., Morford, J.L., Bura-Nakić, E., Breitenbach, S.F., Och, L. (2016) Closing in on the marine $^{238}U/^{235}U$ budget. *Chemical Geology* 420, 11–22. https://doi.org/10.1016/j.chemgeo.2015.10.041

Arthur, M.A., Dean, W.E. (1998) Organic-matter production and preservation and evolution of anoxia in the Holocene Black Sea. *Paleoceanography* 13, 395–411. https://doi.org/10.1029/98PA01161

Broecker, W.S. (1982) Glacial to interglacial changes in ocean chemistry. *Progress in Oceanography* 11, 151–197. https://doi.org/10.1016/0079-6611(82)90007-6

Canfield, D., E., Thamdrup, B. (2009) Towards a consistent classification scheme for geochemical environments, or, why we wish the term 'suboxic' would go away. *Geobiology* 7, 385–392. https://doi.org/10.1111/j.1472-4669.2009.00214.x

Chase, Z., Anderson, R.F., Fleisher, M.Q. (2001) Evidence from authigenic uranium for increased productivity of the glacial Subantarctic Ocean. *Paleoceanography* 16, 468–478. https://doi.org/10.1029/2000PA000542

Chen, X., Romaniello, S.J., Herrmann, A.D., Samankassou, E., Anbar, A.D. (2018a) Biological effects on uranium isotope fractionation ($^{238}U/^{235}U$) in primary biogenic carbonates. *Geochimica et Cosmochimica Acta* 240, 1–10. https://doi.org/10.1016/j.gca.2018.08.028

Chen, X., Romaniello, S.J., Herrmann, A.D., Hardisty, D., Gill, B.C., Anbar, A.D. (2018b) Diagenetic effects on uranium isotope fractionation in carbonate sediments from the Bahamas. *Geochimica et Cosmochimica Acta* 237, 294–311. https://doi.org/10.1016/j.gca.2018.06.026

Cheng, H., Adkins, J.F., Edwards, R.L., Boyle, E.A. (2000) U-Th dating of deep-sea corals. *Geochimica et Cosmochimica Acta* 64, 2401–2416. https://doi.org/10.1016/S0016-7037(99)00422-6

Jaccard, S.L., Galbraith, E.D. (2013) Direct ventilation of the North Pacific did not reach the deep ocean during the last deglaciation. *Geophysical Research Letters* 40, 199–203. https://doi.org/10.1029/2012GL054118

Jacobel, A.W., Anderson, R.F., Jaccard, S.L., McManus, J.F., Pavia, F.J., Winckler, G. (2020) Deep Pacific storage of respired carbon during the last ice age: Perspectives from bottom water oxygen reconstructions. *Quaternary Science Reviews* 230, 106065. https://doi.org/10.1016/j.quascirev.2019.106065

Keir, R.S. (1988) On the Late Pleistocene ocean geochemistry and circulation. *Paleoceanography* 3, 413–445. https://doi.org/10.1029/PA003i004p00413

Kipp, M.A., Tissot, F.L.H. (2022) Inverse methods for consistent quantification of seafloor anoxia using uranium isotope data from marine sediments. *Earth and Planetary Science Letters* 577, 117240. https://doi.org/10.1016/j.epsl.2021.117240

Kipp, M.A., Li, H., Ellwood, M.J., John, S.G., Middag, R., Adkins, J.F., Tissot, F.L.H. (2022) ^{238}U, ^{235}U and ^{234}U in seawater and deep-sea corals: A high-precision reappraisal. *Geochimica et Cosmochimica Acta* 336, 231–248. https://doi.org/10.1016/j.gca.2022.09.018

Ku, T.-L., Knauss, K.G., Mathieu, G.G. (1977) Uranium in open ocean: concentration and isotopic composition. *Deep Sea Research* 24, 1005–1017. https://doi.org/10.1016/0146-6291(77)90571-9

Lau, K.V., Lyons, T.W., Maher, K. (2020) Uranium reduction and isotopic fractionation in reducing sediments: Insights from reactive transport modeling. *Geochimica et Cosmochimica Acta* 287, 65–92. https://doi.org/10.1016/j.gca.2020.01.021

Lomitschka, M., Mangini, A. (1999) Precise Th/U-dating of small and heavily coated samples of deep sea corals. *Earth and Planetary Science Letters* 170, 391–401. https://doi.org/10.1016/S0012-821X(99)00117-X

McManus, J., Berelson, W.M., Klinkhammer, G.P., Hammond, D.E., Holm, C. (2005) Authigenic uranium: relationship to oxygen penetration depth and organic carbon rain. *Geochimica et Cosmochimica Acta* 69, 95–108. https://doi.org/10.1016/j.gca.2004.06.023

Morford, J.L., Emerson, S. (1999) The geochemistry of redox sensitive trace metals in sediments. *Geochimica et Cosmochimica Acta* 63, 1735–1750. https://doi.org/10.1016/S0016-7037(99)00126-X

Riedinger, N., Scholz, F., Abshire, M.L., Zabel, M. (2021) Persistent deep water anoxia in the eastern South Atlantic during the last ice age. *Proceedings of the National Academy of Sciences*. Proceedings of the National Academy of Sciences 118, e2107034118. https://doi.org/10.1073/pnas.2107034118

Romaniello, S.J., Herrmann, A.D., Anbar, A.D. (2013) Uranium concentrations and $^{238}U/^{235}U$ isotope ratios in modern carbonates from the Bahamas: Assessing a novel paleoredox proxy. *Chemical Geology* 362, 305–316. https://doi.org/10.1016/j.chemgeo.2013.10.002

Sarmiento, J.L., Toggweiler, J.R. (1984) A new model for the role of the oceans in determining atmospheric pCO_2. *Nature* 308, 621. https://doi.org/10.1038/308621a0

Shakun, J.D., Clark, P.U., He, F., Marcott, S.A., Mix, A.C., Liu, Z., Otto-Bliesner, B., Schmittner, A., Bard, E. (2012) Global warming preceded by increasing carbon dioxide concentrations during the last deglaciation. *Nature* 484, 49. https://doi.org/10.1038/nature10915

Shen, G.T., Boyle, E.A. (1988) Determination of lead, cadmium and other trace metals in annually-banded corals. *Chemical Geology* 67, 47–62. https://doi.org/10.1016/0009-2541(88)90005-8

Sigman, D.M., Boyle, E.A. (2000) Glacial/interglacial variations in atmospheric carbon dioxide. *Nature* 407, 859. https://doi.org/10.1038/35038000

Sigman, D.M., Hain, M.P., Haug, G.H. (2010) The polar ocean and glacial cycles in atmospheric CO_2 concentration. *Nature* 466, 47. https://doi.org/10.1038/nature09149

Tissot, F.L.H., Dauphas, N. (2015) Uranium isotopic compositions of the crust and ocean: Age corrections, U budget and global extent of modern anoxia. *Geochimica et Cosmochimica Acta* 167, 113–143. https://doi.org/10.1016/j.gca.2015.06.034

Tissot, F.L.H., Chen, C., Go, B., Naziemiec, M., Healy, G., Bekker, A., Swart, P.K., Dauphas, N. (2018) Controls of eustasy and diagenesis on the $^{238}U/^{235}U$ of carbonates and evolution of the seawater ($^{234}U/^{238}U$) during the last 1.4 Myr. *Geochimica et Cosmochimica Acta* 242, 233–265. https://doi.org/10.1016/j.gca.2018.08.022

Wang, Y., Costa, K.M., Lu, W., Hines, S.K.V., Nielsen, S.G. (2024) Global oceanic oxygenation controlled by the Southern Ocean through the last deglaciation. *Science Advances* 10, eadk2506. https://doi.org/10.1126/sciadv.adk2506

Yarincik, K.M., Murray, R.W., Lyons, T.W., Peterson, L.C., Haug, G.H. (2000) Oxygenation history of bottom waters in the Cariaco Basin, Venezuela, over the past 578,000 years: Results from redox-sensitive metals (Mo, V, Mn, and Fe). *Paleoceanography* 15, 593–604. https://doi.org/10.1029/1999PA000401

Zhang, F., Lenton, T.M., del Rey, A., Romaniello, S.J., Chen, X., Planavsky, N.J., Clarkson, M.O., Dahl, T.W., Lau, K.V., Wang, W., Li, Z., Zhao, M., Isson, T., Algeo, T.J., Anbar, A.D. (2020) Uranium isotopes in marine carbonates as a global ocean paleoredox proxy: A critical review. *Geochimica et Cosmochimica Acta* 287, 27–49. https://doi.org/10.1016/j.gca.2020.05.011

Zhou, Y., McManus, J.F. (2023) Authigenic uranium deposition in the glacial North Atlantic: Implications for changes in oxygenation, carbon storage, and deep water-mass geometry. *Quaternary Science Reviews* 300, 107914. https://doi.org/10.1016/j.quascirev.2022.107914

© 2024 The Authors
Published by the European Association of Geochemistry

$^{238}U/^{235}U$ in deep-sea corals reflects limited expansion of seafloor anoxia in last ice age

M.A. Kipp, A. Gao, J.F. Adkins, F.L.H. Tissot

Supplementary Information

The Supplementary Information includes:

- Samples
- Methods
- Tables S-1 to S-9
- Figures S-1 to S-3
- Supplementary Information References

Samples

We studied cold-water scleractinian corals, *Desmophyllum dianthus* (hereafter *D. dianthus*). Samples were previously collected from the New England (Robinson *et al.*, 2007) and Tasmanian (Thiagarajan *et al.*, 2013) seamounts. We analysed a total of 74 fossil corals (n = 32 Atlantic, n = 42 Pacific) ranging in age from 118 to 218,494 yr (***Tables S-1 to S-3***). Eight Atlantic corals were sub-sampled and analysed 4 times each following different cleaning protocols, giving a total of 98 fossil coral U isotope analyses (n = 56 Atlantic, n = 42 Pacific).

Methods

Cleaning tests

Because the time interval investigated is short (~220 kyr) relative to the marine U residence time (~400 kyr), and changes in seafloor anoxic area may have been subtle, changes in seawater $\delta^{238}U$ values in response to fluctuations of the oceanic redox conditions were expected to be small, if at all present. We therefore performed a series of cleaning tests on fossil corals to ensure that isotopic signatures would not be contaminated by exogenous U sources (namely FeMn crusts, organic material, and detrital grains; ***Table S-4***). All lab work was performed at the Isotoparium (Caltech) and all acids used were purchased Optima grade or were twice distilled.

For 8 corals spanning the age range of the dataset (7.1 to 218.5 kyr; ***Table S-1***), large septa were cut using a Dremel tool and physically cleaned by abrasion with a razor blade to remove as much FeMn-oxide coating as possible. For samples with smaller septa, multiple adjacent septa were removed at once to obtain sufficient mass for high-precision U isotope work. An attempt was made to keep the coral fragments as large and intact as possible throughout the physical cleaning step.

After physical cleaning, each of the 8 septa was broken into four similar-sized subsamples (***Fig. S-1***), weighed, and separated into clean PFA vials to undergo different chemical cleaning procedures (***Table S-5***). An assumption was made that these four pieces had the same U concentration and isotopic composition (Kipp *et al.*, 2022), though intra-sample $^{234}U/^{238}U$ heterogeneity (Robinson *et al.*, 2006) likely persists in these subsamples (despite their large size), and thus may impact the observed trends.

Four chemical cleaning treatments were investigated in this study (***Table S-5***). These were derived from well-established protocols used previously in the literature (Boyle, 1981; Boyle and Keigwin, 1985; Cheng *et al.*, 2000; Shen and Boyle, 1988). Because prior work has shown that oxidative cleaning steps can effectively remove FeMn oxide coatings (by degrading the organic matter that "glues" FeMn crusts to corals; Cheng *et al.*, 2000), reductive cleaning steps were not explored in this study (***Table S-5***). The four treatments thus comprise a range of physical to oxidative chemical pre- and post-powdering cleaning steps (***Fig. S-2***).

The first treatment (Treatment A) involved only the first step of the cleaning procedure reviewed in Cheng *et al*. (2000). Each vial was filled with enough Milli-Q water (hereafter MQ-H_2O) to submerge the sample (typically ~10 mL), capped and sonicated for 20 min. The supernatant was then discarded and the procedure repeated 3 times (in total), after which the samples were left to dry in a laminar flow hood for ~ 8 hr. The goal of this approach was to remove only the most readily labile U (*i.e.*, adsorbed or physically trapped on the surface), without mobilisation of elements bound to the crystal structure.

In the second approach (Treatment B), two additional “pre-cleaning” (*i.e.*, before powdering samples) steps were performed (***Table S-5***). The first was submersion in methanol (~10 mL) and sonication for 20 min, to dislodge any fine material loosened by the physical cleaning step (Boyle, 1981). This sonication step was repeated 3 times, after which the samples were left to dry in a laminar flow hood for a few hours. Next, the samples were submerged in a 1:1 30% H_2O_2 and 1 M NaOH solution to oxidise organic material attached to the surface layers of the coral samples and release FeMn crusts “glued” to the coral by these organics (Cheng *et al.*, 2000). The samples were left to react in the solution until the reaction stopped (as evidenced by cessation of bubbling), which was ~ 24 hr. Finally, the samples were rinsed with MQ-H_2O and left to dry in a laminar flow hood for ~ 8 hr.

The third (Treatment C) treatment involved all the chemical cleaning steps in the pre-cleaning procedure of Cheng *et al*. (2000). In order, that includes the MQ-H_2O sonication, an H_2O_2 + NaOH solution treatment, the methanol and sonication, an H_2O_2 and $HClO_4$ solution treatment, and one last MQ-H_2O sonication (***Table S-5***). For the H_2O_2 and NaOH solution treatment, we used a 1:1 ratio of 30 % H_2O_2 and 1 M NaOH. The samples were left in the solution for a total of 60 min with no sonication during this time. For the H_2O_2 and $HClO_4$ solution treatment, we used a 1:1 ratio of 30 % H_2O_2 and 2 % of concentrated $HClO_4$. The samples were left in this solution for a total of 3 min with no sonication. Enough solution was added to fully submerge the samples. For the final MQ-H_2O rinse, the beakers were filled with MQ-H_2O and sonicated for 3 min. This was repeated three times, then the samples were left to dry in a laminar flow hood for ~8 hr.

After cleaning and drying, the 32 sub-samples were powdered with an agate mortar and pestle. The powders were then transferred to plastic centrifuge tubes and weighed once more before only the samples in Treatment D underwent the post-powdering cleaning.

Treatment D included all steps of Treatment C as well as six extra steps after samples were powdered, modified from Shen and Boyle (1988). The powders were first submerged in MQ-H_2O and sonicated for 5 min. This step was repeated 3 times. In between each iteration, the samples were centrifuged and the supernatant was decanted. The centrifuge tubes were then filled with methanol and sonicated for 2 min. This step, including centrifuging, was repeated 3 times. Next, the samples were submerged in 2 % (v/v) twice-distilled HNO_3 for a total of 90 s. The MQ-H_2O sonication step was then repeated three times again. Next, a 1:1 solution of 30 % H_2O_2 and 1 M NaOH was added. The sample was left to react with this oxidant-base solution for 20 min. Finally, the MQ-H_2O sonication step was repeated three more times to remove any trace of acid. The final powders were left to dry in a laminar flow hood.

Elemental and Isotopic analyses

The powdered (and cleaned, in the case of Treatment D) samples were dissolved in excess 20 % (v/v; ~3.5 M) glacial acetic acid to digest coral aragonite while sparing non-carbonate phases (*e.g.*, Tissot *et al.*, 2018). Each sample was spiked with the IRMM-3636 ^{233}U-^{236}U double spike (Verbruggen *et al.*, 2008) such that U_{spike}/U_{sample} was ~3 % (Tissot *et al.*, 2019). To monitor long-term external reproducibility, several powder aliquots of geostandard BCR-2 were prepared alongside the coral samples.

Major and trace element concentrations were analysed on an iCAP RQ ICP-MS (ThermoFisher) following methods previously established at Caltech (Chen *et al.*, 2021, 2023). An aliquot was taken from the bulk digest to check the [Ca^{2+}] concentration via monitoring the ^{48}Ca signal intensity. Solutions were then prepared to a uniform [Ca^{2+}] concentration in the range of 1-10 mM (higher concentrations were utilized for analyses of trace constituents). These solutions were then bracketed by NIST RM 8301C (Stewart *et al.*, 2021) diluted to the same [Ca^{2+}] concentration. Each sample and standard analysis included ^{7}Li, ^{11}B, ^{24}Mg, ^{25}Mg, ^{27}Al, ^{43}Ca, ^{48}Ca, ^{55}Mn, ^{57}Fe, ^{58}Fe, ^{87}Sr, ^{88}Sr, ^{111}Cd, ^{138}Ba, ^{232}Th and ^{238}U. All analyses were cast as element/calcium ratios (with the exception of Li/Mg), and the bracketing concentration-matched NIST RM 8301C was used to correct sample ratios. A well-characterized coral standard (Jcp-1; Hathorne *et al.*, 2013) was treated as a sample and analysed multiple times to establish analytical precision and accuracy. The values obtained (***Table S-6***) agree well with prior work (Hathorne *et al.*, 2013; Chen *et al.*, 2023).

A prepFAST MC ion exchange chromatography system was used to isolate U from matrix elements using UTEVA resin following published methods (Tissot and Dauphas, 2015). Chemical purification was performed twice to ensure minimal matrix (particularly Ca) content in the final solution, which could impact the accuracy of the $^{234}U/^{238}U$ data (Tissot *et al.*, 2018).

All isotopic measurements were made on the NeptunePlus multiple collector inductively coupled plasma mass spectrometer (MC-ICP-MS) at the Isotoparium. The $^{238}U/^{235}U$ ratios are reported as $\delta^{238}U$ values in units of permil relative to CRM-112a:

$$\delta^{238}U = \left[\frac{^{238}U/^{235}U_{sample}}{^{238}U/^{235}U_{standard}} - 1\right] \times 1000 \text{ . (S-1)}$$

The $^{234}U/^{238}U$ ratios are reported as the age-corrected initial $\delta^{234}U_{sec}$ value (*i.e.*, $\delta^{234}U_i$), where

$$\delta^{234}U_i = \delta^{234}U_{sec}\ e^{(\lambda_{234}-\lambda_{238})t} \quad \text{(S-2)}$$

and

$$\delta^{234}U_{sec} = \left[\frac{(^{234}U/^{238}U)_{sample}}{(^{234}U/^{238}U)_{SE}} - 1\right] \times 1000 \quad \text{(S-3)}$$

and $(^{234}U/^{238}U)_{SE}$ is the atomic ratio at secular equilibrium, which is equal to the ratio of the decay constants: $\lambda_{238}/\lambda_{234} = (1.5513 \times 10^{-10})/(2.8220 \times 10^{-6}) = 5.4970 \times 10^{-5}$ (Cheng *et al.*, 2013). Here we report the $\delta^{234}U_i$ data from the 32 sub samples of the eight corals in the cleaning test portion of the study; the $\delta^{234}U_i$ data for the remainder of the fossil coral record will be discussed elsewhere. The coral ages used here are all from the literature (Robinson *et al.*, 2007; Thiagarajan *et al.*, 2013; Hines *et al.*, 2015). The analytical uncertainties for U isotope data are expressed as 95 % confidence intervals (95 CI) based on replicate analyses of a sample solution. Replicate measurements ($n_{digests}$ = 2, $n_{analyses}$ = 4) of the BCR-2 basalt geostandard gave an average $\delta^{238}U$ of -0.270 ± 0.035 ‰ and average $\delta^{234}U_{sec}$ of +0.68 ± 0.69 ‰, within the uncertainty of the established values of $\delta^{238}U$ = -0.262 ± 0.004 ‰ (calculated using all previously published high-precision data; Li and Tissot, 2023) and $\delta^{234}U_{sec}$ = +0.64 ± 0.08 ‰ (Kipp *et al.*, 2022). We also note that the close agreement between our fossil data and the modern *D. dianthus* data of Kipp *et al.*, 2022 further suggests that our analyses are accurate within the quoted precision.

Isotope mass balance modelling

We used the inverse isotope mass balance framework of Kipp and Tissot (2022) to estimate the fractional extent of anoxic seafloor (f_{anoxic}) through the last 60 kyr where our record is most dense. The parameterisation was slightly updated to account for new constraints on seawater U isotopic composition (Kipp *et al.*, 2022); a summary of the parameterisation is provided in ***Table S-7***. Since a comprehensive description of the model architecture and inversion scheme is provided in Kipp and Tissot (2022), we provide here only an overview of the salient aspects of the calculations.

The marine U reservoir (N_{sw}) mass balance is first written,

$$\frac{d(N_{sw})}{dt} = J_{riv} - J_{anox} - J_{other} \quad \text{(S-4)}$$

where J_{riv} is the riverine U flux into the ocean and J_{anox} and J_{other} represent U burial in anoxic and non-anoxic sediments, respectively. The seawater U isotope ($\delta^{238}U_{sw}$) mass balance is then expressed as,

$$\frac{d(\delta^{238}U_{sw})}{dt} = \left(J_{riv} * \left(\delta^{238}U_{riv} - \delta^{238}U_{sw}\right) - J_{anox} * \Delta_{anox} - J_{other} * \Delta_{other}\right)/N_{sw} \quad \text{(S-5)}$$

where $\delta^{238}U_{riv}$ is the average U isotopic composition of rivers and Δ_{anox} and Δ_{other} are the isotopic fractionations associated with U burial in anoxic and non-anoxic sediments, respectively. To relate elemental fluxes to seafloor area, fluxes are calculated as

$$J_{anox} = N_{sw} * K_{anox} * f_{anox} \quad \text{(S-6)}$$

$$J_{other} = N_{sw} * K_{other} * (1 - f_{anox}) \quad \text{(S-7)}$$

where f_{anox} and f_{other} are the fractions of the seafloor overlain by anoxic and non-anoxic waters, and K_{anox} and K_{other} are rate constants for U burial in anoxic and non-anoxic sediments, respectively. For the parameter values in ***Table S-7***, the steady state $\delta^{238}U_{sw}$ value is -0.379 ‰, calibrated (by adjusting K_{other}) to match the value determined by Kipp *et al*. (2022).

We also conducted an inversion where f_{anoxic} was held constant at the modern value and a "suboxic" sink (J_{subox}) was added. The updated mass balance equation becomes

$$\frac{d(N_{sw})}{dt} = J_{riv} - J_{anox} - J_{subox} - J_{other} \qquad \text{(S-8)}$$

and updated isotope mass balance equation becomes

$$\frac{d(\delta^{238}U_{sw})}{dt} = \left(J_{riv} * \left(\delta^{238}U_{riv} - \delta^{238}U_{sw}\right) - J_{anox} * \Delta_{anox} - J_{subox} * \Delta_{subox} - J_{other} * \Delta_{other}\right)/N_{sw} \qquad \text{(S-9)}$$

where

$$J_{subox} = N_{sw} * K_{subox} * f_{subox} \qquad \text{(S-10)}$$

We used a K_{subox} value of 1e-5, which is intermediate between the K_{anox} and K_{other} values. While uncertain, varying this value does not appreciably affect the results. The reason is that the Δ_{subox} value (0.1 ‰, following Tissot and Dauphas, 2015; Andersen *et al.*, 2016) is small, meaning the suboxic sink has little isotopic leverage on $\delta^{238}U_{sw}$. As a result, our model tests (***Fig. 3b***) showed that potentially large variations in f_{subox} are possible given the $\delta^{238}U$ data, but we cannot vote for or against such fluctuations based on the $\delta^{238}U$ record alone. In contrast, the inversion results using only the anoxic + non-anoxic sinks constrain potential fluctuations in f_{anox} to being quite small, owing to the larger isotopic effect, as well as more efficient U burial. For both inverse modelling exercises (***Fig. 3***), inferred f_{anoxic} and $f_{suboxic}$ trends are plotted as the median (solid lines) and 16th to 84th percentile confidence intervals (shading).

We further performed forward model runs to test specific scenarios. The parameterisation of these forward model runs can be found in ***Table S-8*** and is discussed in the main text.

Supplementary Tables

Table S-1 Uranium isotopic data from corals subjected to cleaning tests.

Sample	Age (yr)	2se	Depth (m)	$\delta^{238}U$ (‰)	95 CI	$\delta^{234}U_i$ (‰)	95 CI	U (ppm)	n	Treatment
ALV-3890-1643-005-005	7120	356	1487	-0.368	0.025	138.84	0.69	3.13	10	A
				-0.374	0.020	135.66	0.41	3.23	12	B
				-0.381	0.020	135.84	0.41	3.20	12	C
				-0.384	0.029	138.31	0.93	2.74	3	D
ALV-3892-1315-001-010	31296	1565	1713	-0.392	0.017	141.53	1.02	3.79	3	A
				-0.375	0.012	139.94	0.72	5.39	6	B
				-0.394	0.012	139.93	0.72	4.50	6	C
				-0.391	0.017	140.42	1.02	5.07	3	D
ALV-3890-1235-001-002	40361	2018	2004	-0.371	0.029	141.99	1.03	3.12	3	A
				-0.367	0.029	145.89	1.03	2.80	3	B
				-0.378	0.029	144.90	1.03	3.60	3	C
				-0.385	0.029	141.15	1.03	3.42	3	D
ALV-3883-1346-004-003	48700	2435	1506	-0.373	0.017	112.83	1.07	3.15	3	A
				-0.393	0.012	132.42	0.76	2.81	6	B
				-0.391	0.017	123.28	1.07	2.57	3	C
				-0.402	0.021	123.21	1.31	2.70	2	D
ALV-3887-1436-003-007	82297	4115	2441	-0.382	0.021	142.43	1.17	2.78	3	A
				-0.394	0.021	143.58	1.17	2.61	3	B
				-0.383	0.021	143.08	1.17	2.61	3	C
				-0.386	0.021	144.12	1.17	2.54	3	D
ALV-3887-1436-003-006	91181	4559	2441	-0.392	0.021	149.55	1.20	3.65	3	A
				-0.387	0.021	146.21	1.20	4.33	3	B
				-0.365	0.021	146.80	1.20	3.98	3	C
				-0.390	0.017	147.56	1.21	3.50	3	D
ALV-3890-1330-002-006	147233	7362	1886	-0.380	0.029	159.14	1.39	3.10	3	A
				-0.383	0.029	153.76	1.39	2.91	3	B
				-0.374	0.029	155.95	1.39	3.33	3	C
				-0.381	0.029	154.22	1.39	2.81	3	D
ALV-3889-1326-002-B7	218494	10925	1723	-0.369	0.029	191.51	1.70	2.29	3	A
				-0.361	0.029	153.77	1.70	3.23	3	B
				-0.365	0.029	164.31	1.70	1.23	3	C
				-0.368	0.029	180.40	1.70	1.94	3	D

Table S-2 Elemental data from corals subjected to cleaning tests.

Sample	Treatment	Mn/Ca (μmol/mol)	Fe/Ca (μmol/mol)	Mg/Ca (mmol/mol)	Sr/Ca (mmol/mol)	Cd/Ca (μmol/mol)	Ba/Ca (μmol/mol)	Li/Ca (μmol/mol)	B/Ca (μmol/mol)	U/Ca (μmol/mol)
ALV-3890-1643-005-005	A	47.1	26.83	2.57	10.53	0.289	14.37	13.18	675.8	1.55
	B	38.72	16.35	2.38	10.29	0.267	11.8	11.68	773.4	1.58
	C	43.49	38.98	2.4	10.32	0.301	11.34	11.58	771.9	1.59

	D	4.23	19.87	2.43	10.34	0.295	11.51	11.98	754.8	1.65
ALV-3892-	A	2.23	16.32	2.02	10.25	0.41	15.02	11.57	769.1	1.94
1315-001-010	B	5.3	15.48	1.63	10.31	0.49	15.32	9.86	714.5	2.41
	C	1.87	16.37	1.78	10.25	0.48	15.71	10.21	725.7	2.3
	D	1.55	16.74	1.82	10.34	0.47	15.55	11.01	659.8	2.31
ALV-3890-	A	7.76	16.2	2.17	10.01	0.1	11.27	9.81	736.2	1.75
1235-001-002	B	5.02	16.64	2.46	10.39	0.09	12.01	11.71	740.1	1.56
	C	2.32	16.54	2.39	10.25	0.09	11.56	11.3	713.3	1.61
	D	3.52	15.18	2.1	9.87	0.09	10.89	9.87	744	1.72
ALV-3883-	A	10.6	17.85	2.03	9.72	0.31	9.33	10.38	730.6	1.65
1346-004-003	B	8.35	19.51	2.45	10	0.3	11.24	13.26	730.1	1.5
	C	12.79	17.36	2.32	9.96	0.3	9.19	12.43	774.7	1.57
	D	57.81	19.75	2.14	9.94	0.27	10.38	11.82	772	1.73
ALV-3887-	A	23.91	26.31	2.11	9.41	0.2	12.72	9.23	662.9	1.36
1436-003-007	B	14.75	14.03	2.12	9.69	0.13	13.92	9.5	679.1	1.43
	C	6.54	21.99	2.02	10.01	0.16	13.34	9.28	682.4	1.46
	D	11.73	14.6	2.11	9.64	0.13	13.67	9.47	645.5	1.39
ALV-3887-	A	7.06	15.48	2.1	10.09	0.16	14.87	9.56	659.2	1.73
1436-003-006	B	5.03	15.87	1.88	9.96	0.17	14.77	8.99	622.5	1.86
	C	1.98	14.88	2.14	9.95	0.17	14.55	9.31	692.2	1.69
	D	4.53	17.86	1.95	9.93	0.36	14.92	9.21	650.7	1.74
ALV-3890-	A	19.88	20.28	2.14	9.95	0.11	10.34	11.43	692	1.43
1330-002-006	B	42.47	14.6	2.18	9.81	0.12	11.03	10.96	667.6	1.37
	C	17.86	12.04	1.95	9.88	0.16	10	10.32	611.7	1.41
	D	9.64	13.77	1.95	9.81	0.12	9.66	10.21	653.3	1.46
ALV-3889-	A	13.15	16.02	2.7	10.19	0.068	8.93	10.82	627.5	1.24
1326-002-B7	B	15.28	16.47	2.08	10.08	0.095	9.34	7.76	657.6	1.7
	C	4.04	17.79	2.5	10.02	0.084	8.81	9.51	700.8	1.41
	D	8.29	19.71	2.63	10.16	0.089	8.11	10.57	737.9	1.33

Table S-3 Uranium isotopic data from all other corals.

Sample	Age (yr)	2se	Depth (m)	$\delta^{238}U$ (‰)	95 CI	U (ppm)	n
ATLANTIC							
ALV-3883-1248-003-003	118	6	1524	-0.371	0.012	3.58	6
ALV-3891-1459-003-013	6251	313	1176	-0.390	0.018	3.36	3
ALV-3891-1459-003-002	11378	569	1176	-0.371	0.012	4.92	6
ALV-3890-1407-003-001	12222	611	1778	-0.385	0.018	2.97	3
ALV-3890-1742-007-001	15825	791	1381	-0.388	0.022	3.84	2
ALV-3890-1643-005-003	17064	853	1487	-0.380	0.018	3.11	3
ALV-3889-1311-001-001	17950	898	1719	-0.388	0.012	4.73	6
ALV-3889-1311-001-003	23438	1172	1719	-0.387	0.019	3.63	3
ALV-3889-1311-001-005	25317	1266	1719	-0.375	0.012	4.04	6
ALV-3889-1311-001-002	26228	1311	1719	-0.381	0.012	4.74	6
ALV-3889-1311-001-006	28712	1436	1719	-0.395	0.012	3.65	6
ALV-3892-1315-001-006	34512	1726	1713	-0.374	0.015	3.84	4
ALV-3892-1711-006-004	39704	1985	1548	-0.381	0.012	3.97	6
ALV-3892-1711-006-010	39896	1995	1548	-0.391	0.018	3.17	3
ALV-3883-1248-003-004	44859	2243	1524	-0.373	0.012	3.86	6
ALV-3885-1520-005-008	49359	2468	1821	-0.384	0.012	4.17	6
ALV-3892-1711-006-002	57068	2853	1548	-0.393	0.012	3.46	6
ALV-3892-1711-006-006	57313	2866	1548	-0.376	0.012	3.72	6
ALV-3885-1452-004-003	58593	2930	1878	-0.388	0.012	4.26	6
ALV-3890-1330-002-005	151351	7568	1886	-0.383	0.022	4.84	2
ALV-3889-1526-006-001	155114	7756	1620	-0.382	0.012	3.50	6
ALV-3885-1520-005-014	161878	8094	1821	-0.372	0.018	4.00	3
ALV-3885-1520-005-007	162741	8137	1821	-0.372	0.012	4.73	6
ALV-3885-1520-005-012	165097	8255	1821	-0.375	0.018	3.60	3
PACIFIC							
TN228-J2-387-1226-2330-25-1448-001	11951	67	1448	-0.405	0.021	3.75	3
TN228-J2-382-1216-1350-03-1523-008	12682	33	1523	-0.385	0.015	3.56	5
TN228-J2-387-1226-1635-23-1599-002	13817	63	1599	-0.385	0.021	4.00	3
TN228-J2-383-1217-0725-01-1575-004	13922	79	1575	-0.402	0.021	4.38	4
TN228-J2-387-1226-1635-23-1599-020	14028	159	1599	-0.378	0.021	5.05	3
TN228-J2-387-1226-1635-23-1599-016	14390	80	1599	-0.388	0.017	4.36	3
TN228-J2-387-1226-1148-20-1680-003	14464	52	1680	-0.387	0.021	6.32	3
TN228-J2-387-1226-0615-17-1748-009	14869	53	1748	-0.381	0.021	4.84	3
TN228-J2-393-0112-0730-13-1442-003	15056	67	1442	-0.387	0.020	4.75	2
TN228-J2-387-1226-0615-17-1748-020	16129	71	1748	-0.394	0.021	6.62	3
TN228-J2-382-1216-1010-01-1689-002	16722	836	1689	-0.383	0.018	4.19	3
TN228-J2-393-0112-0730-13-1442-002	16804	202	1442	-0.369	0.029	3.83	1
TN228-J2-387-1226-0615-17-1748-016	17065	46	1748	-0.383	0.017	6.32	3
TN228-J2-382-1216-1010-01-1689-004	17279	864	1689	-0.390	0.018	3.87	3
TN228-J2-382-1216-1010-01-1689-009	17608	164	1689	-0.379	0.017	4.59	3
TN228-J2-382-1216-1350-03-1523-007	18333	38	1523	-0.375	0.025	4.13	2
TN228-J2-383-1217-1320-05-1460-008	19274	57	1460	-0.369	0.017	4.61	3
TN228-J2-383-1217-0725-01-1575-023	19457	108	1575	-0.363	0.017	6.28	3

TN228-J2-382-1216-1350-03-1523-006	20367	1018	1523	-0.376	0.022	4.43	2
TN228-J2-382-1216-1350-03-1523-005	21344	153	1523	-0.371	0.018	6.05	3
TN228-J2-382-1216-1350-03-1523-003	21704	1085	1523	-0.376	0.018	5.58	3
TN228-J2-395-0114-0057-09-1500-002	23338	75	1500	-0.381	0.021	3.26	3
TN228-J2-395-0114-0057-09-1500-010	25198	144	1500	-0.385	0.021	6.46	3
TN228-J2-395-0114-0057-09-1500-008	25526	209	1500	-0.387	0.021	4.27	3
TN228-J2-382-1216-1350-03-1523-010	25769	1288	1523	-0.387	0.018	3.72	3
TN228-J2-383-1217-0725-01-1575-001	27579	92	1575	-0.381	0.016	5.18	5
TN228-J2-395-0114-0057-09-1500-006	30002	155	1500	-0.363	0.021	2.84	3
TN228-J2-383-1217-0725-01-1575-020	30554	244	1575	-0.382	0.016	4.39	5
TN228-J2-383-1217-0725-01-1575-007	31286	166	1575	-0.402	0.021	4.64	3
TN228-J2-383-1217-0725-01-1575-012	32006	88	1575	-0.369	0.015	4.89	6
TN228-J2-383-1217-0725-01-1575-014	32554	171	1575	-0.387	0.016	5.00	5
TN228-J2-383-1217-0725-01-1575-021	33969	302	1575	-0.384	0.017	4.87	3
TN228-J2-382-1216-1010-01-1689-007	34362	1718	1689	-0.386	0.018	5.02	3
TN228-J2-395-0114-0057-09-1500-005	36678	98	1500	-0.378	0.012	4.71	6
TN228-J2-393-0112-0124-06-1657-011	37141	142	1657	-0.384	0.017	4.30	3
TN228-J2-383-1217-1320-05-1460-005	38061	93	1460	-0.375	0.015	5.10	6
TN228-J2-395-0114-0057-09-1500-009	39702	158	1500	-0.366	0.021	4.29	3
TN228-J2-383-1217-0725-01-1575-005	41443	109	1575	-0.386	0.015	4.90	6
TN228-J2-382-1216-1010-01-1689-008	42443	158	1689	-0.394	0.017	4.20	4
TN228-J2-383-1217-0725-01-1575-022	53903	146	1575	-0.381	0.015	4.92	6
TN228-J2-382-1216-1010-01-1689-001	54834	128	1689	-0.375	0.015	5.17	5
TN228-J2-382-1216-1350-03-1523-004	67480	3374	1523	-0.395	0.018	4.55	3

Table S-4 Common sources of contamination for geochemical analysis of fossil corals. Modified from Holcomb *et al*. (2015).

Contaminant	Cleaning protocol	Treatment	References
Detritus	Physical cleaning (Dremel + razor blade)	A, B, C, D	Boyle (1981), Boyle and Keigwin (1985), Shen and Boyle (1988)
	H_2O rinsing + sonication	A, B, C, D	
	Methanol rinsing + sonication	B, C, D	
Organic matter	Oxidative cleaning – H_2O_2 + NaOH	B, C, D	Boyle and Keigwin (1985), Cheng *et al*. (2000)
	Oxidative cleaning – H_2O_2 + $HClO_4$	C, D	
Adsorbed ions	Weak acid – 1-2 % HNO_3	D	Shen and Boyle (1988)
	Buffer solution – EDTA	Not studied here	Van de Flierdt *et al*. (2010)
Oxide minerals	Reductive agents – NH_2OH	Not studied here	Boyle (1981) ; Shen and Boyle (1988)
	HCl + NH_4OH	Not studied here	
	Reductive agents – hydrazine + ammonium citrate	Not studied here	

Table S-5 Coral cleaning protocols explored in this study.

Step	A	B	C	D
MQ H_2O	×	×	×	×
1:1 1 M NaOH + 30 % H_2O_2		×	×	×
Methanol		×	×	×
1:1 2 % $HClO_4$ + 30 % H_2O_2			×	×
MQ H_2O			×	×
Powder samples	×	×	×	×
MQ H_2O				×
2 % HNO_3				×
Methanol				×
1:1 1 M NaOH + 30 % H_2O_2				×
MQ H_2O				×

Table S-6 Elemental ratio data for Jcp-1 coral standard. Uncertainties are 2SD.

Study	Mg/Ca (mmol/mol)	Sr/Ca (mmol/mol)	Fe/Ca (µmol/mol)	Mn/Ca (µmol/mol)	Ba/Ca (µmol/mol)	Cd/Ca (µmol/mol)	U/Ca (µmol/mol)	Al/Ca (µmol/mol)
Hathorne *et al.* (2013)	4.199 ± 0.130 (*n* = 19)	8.838 ± 0.084 (*n* = 21)			7.465 ± 1.310 (*n* = 10)		1.192 ± 0.090 (*n* = 8)	
Chen *et al.* (2021, 2023)	4.215 ± 0.044 (*n* = 15)	8.692 ± 0.102 (*n* = 15)					1.192 ± 0.012 (*n* = 3)	
This study	4.122 ± 0.066 (*n* = 5)	8.752 ± 0.148 (*n* = 5)	15.354 ± 0.647 (*n* = 5)	2.260 ± 0.824 (*n* = 5)	7.734 ± 0.254 (*n* = 5)	0.035 ± 0.009 (*n* = 5)	1.190 ± 0.125 (*n* = 5)	82.6 ± 3.2 (*n* = 5)

Table S-7 Parameterization of inverse model runs.

Parameter	Description	Value	Reference
J_{riv}	Riverine U flux	42 Mmol/yr	(Dunk *et al.*, 2002)
$\delta^{238}U_{riv}$	Riverine isotopic composition	-0.30 ‰	(Andersen *et al.*, 2016)
K_{anox}	Anoxic rate constant	1.74e-4	(Kipp and Tissot, 2022)
K_{other}	Oxic rate constant	1.88e-6 (without suboxic sink); 1.52e-6 (with suboxic sink)	(Kipp and Tissot, 2022); this study
K_{subox}	Suboxic rate constant	1.00e-5	Between K_{anox} and K_{other}
Δ_{anox}	Anoxic fractionation factor	0.6 ‰	(Zhang *et al.*, 2020)
Δ_{other}	Oxic fractionation factor	0 ‰	(Zhang *et al.*, 2020)
Δ_{subox}	Suboxic fractionation factor	0.1 ‰	(Tissot and Dauphas, 2015; Andersen *et al.*, 2016)

Table S-8 Perturbations explored in forward model runs.

Test	Figure	Perturbation	Sensitivity test
f_{anoxic} expansion at LGM	4A	f_{anoxic} = 1, 2, and 5 % from 25 – 18 ka	
Lower glacial f_{anoxic} due to Black Sea	4B	f_{anoxic} = 0.09 % from 60 – 9 ka	
$f_{suboxic}$ expansion following aU record	4C	$f_{suboxic}$ = 10, 40, and 90 % before 20 ka	Vary Δ_{subox} from 0.1 to 0.2 ‰
J_{riv} expansion during deglaciation	4D	J_{riv} = 84 Mmol/yr from 20 – 10 ka	$\delta^{238}U_{riv}$ = -0.15 ‰ at 20 – 10 ka

Table S-9 Authigenic uranium records compiled in this study.

Site	Location	Depth (m)	*n*	Latitude	Longitude	Reference
V19-30	Equatorial Pacific	3,100	35	-3.4	-83.5	Bradtmiller *et al.* (2010)
RC13-140	Equatorial Pacific	2,200	12	-2.9	-87.8	Bradtmiller *et al.* (2010)
RC11-238	Equatorial Pacific	2,600	12	-1.5	-85.8	Bradtmiller *et al.* (2010)
MD97-2138	Equatorial Pacific	1,900	13	-1.3	146.0	Bradtmiller *et al.* (2010)
ML1208-37BB	Equatorial Pacific	2,800	108	7.0	-161.6	Jacobel *et al.* (2017)
ML1208-31BB	Equatorial Pacific	2,800	289	4.7	-160.1	Jacobel *et al.* (2017)
ML1208-17PC	Equatorial Pacific	2,900	417	0.5	-156.4	Jacobel *et al.* (2017)
ODP-1240	Equatorial Pacific	2,300	86	0.0	-86.5	Jacobel *et al.* (2020)
ODP-846	Equatorial Pacific	3,300	69	-3.4	-90.8	Jacobel *et al.* (2020)
MC1014-8JC	Equatorial Pacific	1,993	240	6.23	-86.04	Hostak (2019)
MV1014-02-17JC	Equatorial Pacific	2,846	453	-0.2	-85.9	Loveley *et al.* (2017)
DY081-GVY005	North Atlantic	1,907	22	58.61	-43.78	Zhou and McManus (2023)
EW93-03-31GGC	North Atlantic	1,796	118	50.57	-46.35	Zhou and McManus (2023)
306-U1313	North Atlantic	3,426	60	41.00	-32.96	Zhou and McManus (2023)
DY081-GVY001	North Atlantic	3,721	77	50.2	-45.5	Zhou and McManus (2023)
EW93-03-37JPC	North Atlantic	3,981	200	43.68	-46.28	Zhou and McManus (2023)
VM22-109	Southern Ocean	733	22	-41.97	0.25	Chase *et al.* (2001)
TN057-20	Southern Ocean	1,312	27	-41.10	0.60	Chase *et al.* (2001)
RC13-254	Southern Ocean	3,636	77	-48.57	5.12	Kumar *et al.* (1995)
MD84-527	Southern Ocean	3,269	30	-43.83	51.32	Francois *et al.* (1993)
TN057-13PC	Southern Ocean	2,848	40	-53.2	5.1	Jaccard *et al.* (2016)
TN057-14PC	Southern Ocean	3,648	225	-52.0	4.5	Jaccard *et al.* (2016)
ODP-882	North Pacific	3,244	103	50.35	167.58	Jaccard *et al.* (2009)
ODP-887	North Pacific	3,647	46	54.37	-148.45	Galbraith *et al.* (2007)
PC13	North Pacific	2,393	27	49.72	168.30	Jaccard and Galbraith (2013)
EW0408-85JC	North Pacific	682	101	59.6	-144.2	Addison *et al.* (2012)

Supplementary Figures

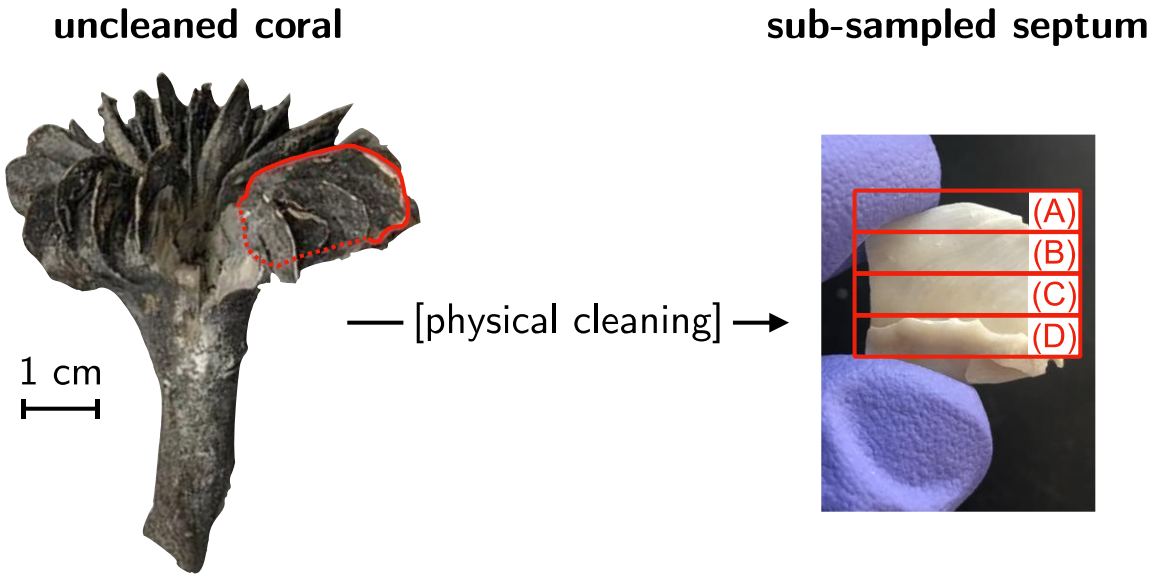

Figure S-1 Example of coral sampling for cleaning tests.

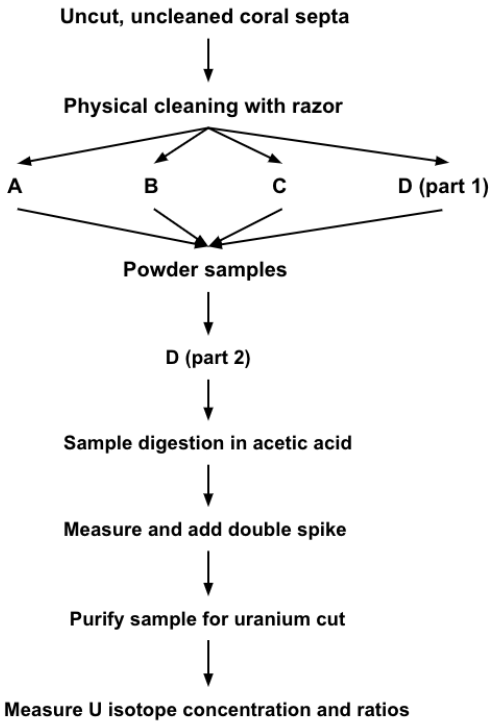

Figure S-2 Flowchart of full protocol for chemical cleaning tests and subsequent isotopic analyses.

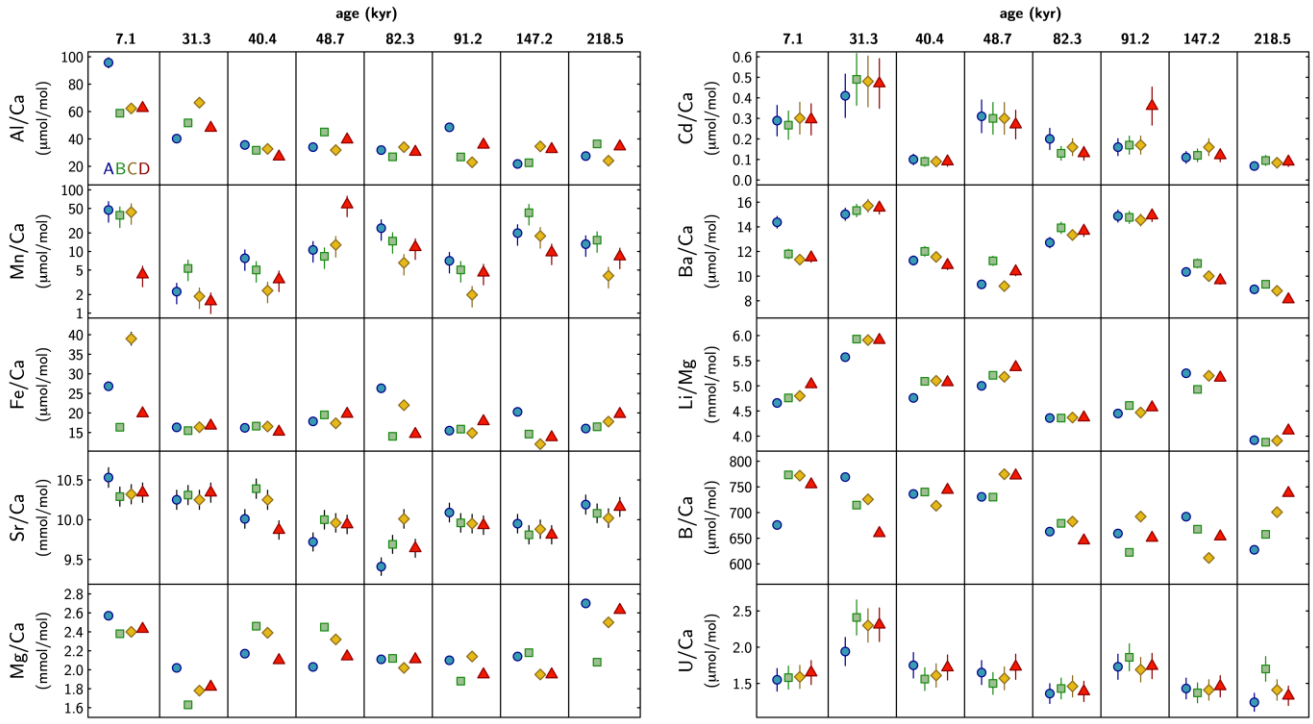

Figure S-3 Major and trace element ratios as a function of cleaning treatment. Symbols denote cleaning Treatments A-D as in Figure 1. Error bars are 1σ; where not visible, uncertainty is less than width of symbol.

Supplementary Information References

Addison, J.A., Finney, B.P., Dean, W.E., Davies, M.H., Mix, A.C., Stoner, J.S., Jaeger, J.M. (2012) Productivity and sedimentary $\delta^{15}N$ variability for the last 17,000 years along the northern Gulf of Alaska continental slope. *Paleoceanography* 27, 2011PA002161. https://doi.org/10.1029/2011PA002161

Andersen, M.B., Vance, D., Morford, J.L., Bura-Nakić, E., Breitenbach, S.F., Och, L. (2016) Closing in on the marine $^{238}U/^{235}U$ budget. *Chemical Geology* 420, 11–22. https://doi.org/10.1016/j.chemgeo.2015.10.041

Boyle, E.A. (1981) Cadmium, zinc, copper, and barium in foraminifera tests. *Earth and Planetary Science Letters* 53, 11–35. https://doi.org/10.1016/0012-821X(81)90022-4

Boyle, E.A., Keigwin, L.D. (1985) Comparison of Atlantic and Pacific paleochemical records for the last 215,000 years: Changes in deep ocean circulation and chemical inventories. *Earth and Planetary Science Letters* 76, 135–150. https://doi.org/10.1016/0012-821X(85)90154-2

Bradtmiller, L.I., Anderson, R.F., Sachs, J.P., Fleisher, M.Q. (2010) A deeper respired carbon pool in the glacial equatorial Pacific Ocean. *Earth and Planetary Science Letters* 299, 417–425. https://doi.org/10.1016/j.epsl.2010.09.022

Chase, Z., Anderson, R.F., Fleisher, M.Q. (2001) Evidence from authigenic uranium for increased productivity of the glacial Subantarctic Ocean. *Paleoceanography* 16, 468–478. https://doi.org/10.1029/2000PA000542

Chen, S., Littley, E.F., Rae, J.W., Charles, C.D., Adkins, J.F. (2021) Uranium Distribution and Incorporation Mechanism in Deep-Sea Corals: Implications for Seawater [CO_3^{2-}] Proxies. *Frontiers in Earth Science* 9, 159. https://doi.org/10.3389/feart.2021.641327

Chen S., Littley, E.F., Rae, J.W., Charles, C.D., Guan, Y., Adkins J.F. (2023) Coherent tracer correlations in deep-sea corals and implications for biomineralization mechanisms underlying vital effects. *Geochimica et Cosmochimica Acta* 343, 304–322. https://doi.org/10.1016/j.gca.2022.12.006

Cheng, H., Adkins, J.F., Edwards, R.L., Boyle, E.A. (2000) U-Th dating of deep-sea corals. *Geochimica et Cosmochimica Acta* 64, 2401–2416. https://doi.org/10.1016/S0016-7037(99)00422-6

Cheng, H., Edwards, R.L., Shen, C.C., Polyak, V.J., Asmerom, Y., Woodhead, J., Hellstrom, J., Wang, Y., Kong, X., Spötl, C., Wang, X., Alexander Jr., E.C. (2013) Improvements in ^{230}Th dating, ^{230}Th and ^{234}U half-life values, and U–Th isotopic measurements by multi-collector inductively coupled plasma mass spectrometry. *Earth and Planetary Science Letters* 371, 82–91. https://doi.org/10.1016/j.epsl.2013.04.006

Dunk, R.M., Mills, R.A., Jenkins, W.J. (2002) A reevaluation of the oceanic uranium budget for the Holocene. *Chemical Geology* 190, 45–67. https://doi.org/10.1016/S0009-2541(02)00110-9

Francois, R., Bacon, M.P., Altabet, M.A., Labeyrie, L.D. (1993) Glacial/interglacial changes in sediment rain rate in the SW Indian Sector of subantarctic Waters as recorded by ^{230}Th, ^{231}Pa, U, and $\delta^{15}N$. *Paleoceanography* 8, 611–629. https://doi.org/10.1029/93PA00784

Galbraith, E.D., Jaccard, S.L., Pedersen, T.F., Sigman, D.M., Haug, G.H., Cook, M., Southon, J.R., Francois, R. (2007) Carbon dioxide release from the North Pacific abyss during the last deglaciation. *Nature* 449, 890–893. https://doi.org/10.1038/nature06227

Hathorne, E.C., Gagnon, A., Felis, T., Adkins, J.F., Asami, R., Boer, W., Caillon, N., Case, D., Cobb, K.M., Douville, E. (2013) Interlaboratory study for coral Sr/Ca and other element/Ca ratio measurements. *Geochemistry, Geophysics, Geosystems* 14, 3730–3750. https://doi.org/10.1002/ggge.20230

Hines, S.K., Southon, J.R., Adkins, J.F. (2015) A high-resolution record of Southern Ocean intermediate water radiocarbon over the past 30,000 years. *Earth and Planetary Science Letters* 432, 46–58. https://doi.org/10.1016/j.epsl.2015.09.038

Holcomb, M., DeCarlo, T.M., Schoepf, V., Dissard, D., Tanaka, K., Mcculloch, M. (2015) Cleaning and pre-treatment procedures for biogenic and synthetic calcium carbonate powders for determination of elemental and boron isotopic compositions. *Chemical Geology* 398, 11–21. https://doi.org/10.1016/j.chemgeo.2015.01.019

Hostak, R.M. (2019) The Connection Between Deep Eastern Equatorial Pacific Ocean Oxygenation and Atmospheric CO_2 Over the Past 180 KYR. PhD Thesis. Texas A&M University.

Jaccard, S.L., Galbraith, E.D. (2013) Direct ventilation of the North Pacific did not reach the deep ocean during the last deglaciation. *Geophysical Research Letters* 40, 199–203. https://doi.org/10.1029/2012GL054118

Jaccard, S.L., Galbraith, E.D., Martínez-García, A., Anderson, R.F. (2016) Covariation of deep Southern Ocean oxygenation and atmospheric CO_2 through the last ice age. *Nature* 530, 207. https://doi.org/10.1038/nature16514

Jaccard, S.L., Galbraith, E.D., Sigman, D.M., Haug, G.H., Francois, R., Pedersen, T.F., Dulski, P., Thierstein, H.R. (2009) Subarctic Pacific evidence for a glacial deepening of the oceanic respired carbon pool. *Earth and Planetary Science Letters* 277, 156–165. https://doi.org/10.1016/j.epsl.2008.10.017

Jacobel, A.W., McManus, J.F., Anderson, R.F., Winckler, G. (2017) Repeated storage of respired carbon in the equatorial Pacific Ocean over the last three glacial cycles. *Nature Communications* 8, 1727. https://doi.org/10.1038/s41467-017-01938-x

Jacobel, A.W., Anderson, R.F., Jaccard, S.L., McManus, J.F., Pavia, F.J., Winckler, G. (2020) Deep Pacific storage of respired carbon during the last ice age: Perspectives from bottom water oxygen reconstructions. *Quaternary Science Reviews* 230, 106065. https://doi.org/10.1016/j.quascirev.2019.106065

Kipp, M.A., Tissot, F.L.H. (2022) Inverse methods for consistent quantification of seafloor anoxia using uranium isotope data from marine sediments. *Earth and Planetary Science Letters* 577, 117240. https://doi.org/10.1016/j.epsl.2021.117240

Kipp, M.A., Li, H., Ellwood, M.J., John, S.G., Middag, R., Adkins, J.F., Tissot, F.L.H. (2022) ^{238}U, ^{235}U and ^{234}U in seawater and deep-sea corals: A high-precision reappraisal. *Geochimica et Cosmochimica Acta* 336, 231–248. https://doi.org/10.1016/j.gca.2022.09.018

Kumar, N., Anderson, R.F., Mortlock, R.A., Froelich, P.N., Kubik, P., Dittrich-Hannen, B., Suter, M. (1995) Increased biological productivity and export production in the glacial Southern Ocean. *Nature* 378, 675. https://doi.org/10.1038/378675a0

Li, H., Tissot, F.L.H. (2023) UID: The uranium isotope database. *Chemical Geology* 618, 121221. https://doi.org/10.1016/j.chemgeo.2022.121221

Loveley, M.R., Marcantonio, F., Wisler, M.M., Hertzberg, J.E., Schmidt, M.W., Lyle, M. (2017) Millennial-scale iron fertilization of the eastern equatorial Pacific over the past 100,000 years. *Nature Geoscience* 10, 760–764. https://doi.org/10.1038/ngeo3024

Robinson, L.F., Adkins, J.F., Fernandez, D.P., Burnett, D.S., Wang, S.-L., Gagnon, A.C., Krakauer, N. (2006) Primary U distribution in scleractinian corals and its implications for U series dating. *Geochemistry, Geophysics, Geosystems* 7, Q05022. https://doi.org/10.1029/2005GC001138

Robinson, L.F., Adkins, J.F., Scheirer, D.S., Fernandez, D.P., Gagnon, A., Waller, R.G. (2007) Deep-sea scleractinian coral age and depth distributions in the northwest Atlantic for the last 225,000 years. *Bulletin of Marine Science* 81, 371–391.

Shen, G.T., Boyle, E.A. (1988) Determination of lead, cadmium and other trace metals in annually-banded corals. *Chemical Geology* 67, 47–62. https://doi.org/10.1016/0009-2541(88)90005-8

Stewart, J.A., Christopher, S.J., Kucklick, J.R., Bordier, L., Chalk, T.B., Dapoigny, A., Douville, E., Foster G.L., Gray, W.R., Greenop, R. (2021) NIST RM 8301 boron isotopes in marine carbonate (simulated coral and foraminifera solutions): inter-laboratory $\delta^{11}B$ and trace element ratio value assignment. *Geostandards and Geoanalytical Research* 45, 77–96. https://doi.org/10.1111/ggr.12363

Thiagarajan, N., Gerlach, D., Roberts, M.L., Burke, A., McNichol, A., Jenkins, W.J., Subhas, A.V., Thresher, R.E., Adkins, J.F. (2013) Movement of deep-sea coral populations on climatic timescales. *Paleoceanography and Paleoclimatology* 28, 227–236. https://doi.org/10.1002/palo.20023

Tissot, F.L.H., Dauphas, N. (2015) Uranium isotopic compositions of the crust and ocean: Age corrections, U budget and global extent of modern anoxia. *Geochimica et Cosmochimica Acta* 167, 113–143. https://doi.org/10.1016/j.gca.2015.06.034

Tissot, F.L.H., Chen, C., Go, B., Naziemiec, M., Healy, G., Bekker, A., Swart, P.K., Dauphas, N. (2018) Controls of eustasy and diagenesis on the $^{238}U/^{235}U$ of carbonates and evolution of the seawater ($^{234}U/^{238}U$) during the last 1.4 Myr. *Geochimica et Cosmochimica Acta* 242, 233–265. https://doi.org/10.1016/j.gca.2018.08.022

Tissot, F.L.H., Ibanez-Mejia, M., Boehnke, P., Dauphas, N., McGee, D., Grove, T.L., Harrison, T.M. (2019) $^{238}U/^{235}U$ measurement in single-zircon crystals: implications for the Hadean environment, magmatic differentiation and geochronology. *Journal of Analytical Atomic Spectrometry* 34, 2035–2052. https://doi.org/10.1039/C9JA00205G

Van de Flierdt, T., Robinson, L.F., Adkins, J.F. (2010) Deep-sea coral aragonite as a recorder for the neodymium isotopic composition of seawater. *Geochimica et Cosmochimica Acta* 74, 6014–6032. https://doi.org/10.1016/j.gca.2010.08.001

Verbruggen, A., Alonso, A., Eykens, R., Kehoe, F., Kuhn, H., Richter, S., Aregbe, Y. (2008) Preparation and certification of IRMM-3636, IRMM-3636a and IRMM-3636b. JRC Scientific and Technical Reports.

Zhang, F., Lenton, T.M., del Rey, A., Romaniello, S.J., Chen, X., Planavsky, N.J., Clarkson, M.O., Dahl, T.W., Lau, K.V., Wang, W., Li, Z., Zhao, M., Isson, T., Algeo, T.J., Anbar, A.D. (2020) Uranium isotopes in marine carbonates as a global ocean paleoredox proxy: A critical review. *Geochimica et Cosmochimica Acta* 287, 27–49. https://doi.org/10.1016/j.gca.2020.05.011

Zhou, Y., McManus, J.F. (2023) Authigenic uranium deposition in the glacial North Atlantic: Implications for changes in oxygenation, carbon storage, and deep water-mass geometry. *Quaternary Science Reviews* 300, 107914. https://doi.org/10.1016/j.quascirev.2022.107914